Engineering of triply entangled states in a single-neutron system

Yuji Hasegawa,[1,2] Rudolf Loidl,[1,3] Gerald Badurek,[1] Katharina Durstberger-Rennhofer,[1] Stephan Sponar,[1] and Helmut Rauch[1,3]

[1]*Atominstitut der Österreichischen Universitäten, Stadionallee 2, A-1020 Wien, Austria*

[2]*PRESTO, Japan Science and Technology Agency (JST), Kawaguchi, Saitama, Japan*

[3]*Institut Laue-Langevin, Boîte Postale 156, F-38042 Grenoble Cedex 9, France*

(Received 4 August 2009; published 25 March 2010)

Entanglement between degrees of freedom, namely between the spin, path, and (total) energy degrees of freedom, in a single-neutron system is exploited. We implemented a triply entangled Greenberger-Horne-Zeilinger (GHZ)–like state and coherently manipulated relative phases of two-level quantum subsystems. An equality derived by Mermin was applied to analyze the generated GHZ-like state: We determined the four expectation values and finally obtained $M = 2.558 \pm 0.004 \not\leqslant 2$. This demonstrates a violation of Mermin-like inequality for triply entangled GHZ-like state in a single-particle system, which, in turn, clearly contradicts the noncontextual assumption and confirms quantum contextuality.

DOI: 10.1103/PhysRevA.81.032121 PACS number(s): 03.65.Ud, 03.67.Bg, 03.75.Dg, 42.50.Dv

I. INTRODUCTION

Einstein, Podolsky, and Rosen argued that quantum mechanics (QM) is not a complete theory in the sense that some results that can be predicted from remote measurements are not described by the theory [1]. Bell showed that local hidden variable theories (LHVTs) satisfy some inequalities that are violated by QM [2,3], and thus QM cannot be completed with LHVTs. Experimental violations of Bell inequalities on bipartite systems have been observed with two-photon [4], two-ion [5], atom-photon [6], and two-hadron [7] systems. Moreover, Bell-like inequalities can be tested using different degrees of freedom of single-particle systems. In this scenario, the violation of the inequality does not prove the impossibility of LHVTs but does prove the impossibility of noncontextual hidden variable theories (NCHVTs) [8,9] (see also [10]). In NCHVTs, the result of a measurement $\hat{A}$ is predetermined and is not affected by other previous (or simultaneous) measurements, carried out on the same individual system, of any observables mutually commuting with $\hat{A}$. Using the spin and path degrees of freedom of single neutrons [11], violations of Bell-like inequalities in a single-particle system have been experimentally confirmed [12]. The spin (polarization) path entanglement of another quantum system, namely of single photons, is reported to be utilized for a demonstration of quantum contextuality [13].

Even more apparent conflicts between predictions by QM and LHVTs were found by Greenberger, Horne, and Zeilinger: entangled states of three or more separated systems can lead to nonstatistical predictions in contradiction to each other [14,15]. Indeed, Mermin showed that this conflict can be converted into a larger violation of a Bell-like inequality between three or more separated systems [16]. Experimental tests of these inequalities were reported, for example, with the use of three and four photons [17,18] and four ions [19]. Among these, tests of quantum nonlocality on many-particle generalizations of the GHZ triplet are particularly appealing [20]. A natural question is whether a violation of Mermin-like inequalities can be observed also on single-particle systems. The interest of this violation goes beyond the technical challenge of preparing GHZ-like entangled states using three degrees of freedom of a single-particle system and the capability of measuring the corresponding observables. The violation of the Mermin-like inequality is interesting in itself because it is more robust to noise (or rather disturbances) than previous violations of bipartite Bell-like inequalities and thus emphasizes the conflict between QM and NCHVTs.

Starting from a demonstration of a violation of Bell-like inequality [12], several neutron optical experiments were accomplished using Bell-like states, with entanglement of two (i.e., the spin and the path) degrees of freedom of neutrons [21,22]. Recently we developed a coherent-manipulation method of a neutron's energy, i.e., total energy of neutrons given by the sum of kinematic and potential energies [23]. This technique accompanied by phase manipulations [24] allows us to add one more degree of freedom to be entangled: a triply entangled GHZ-like state in a single-neutron system is generated and manipulated. Here we report the preparation of a GHZ-like state using three degrees of freedom of a single neutron, that is, two internal degrees of freedom (the spin and the energy) and one external one (the path taken by the neutron in an interferometer setup). In addition, we demonstrate the violation of a Mermin-like inequality with a single-particle system. General descriptions of perfect crystal neutron interferometer experiments can be found in Ref. [25].

II. THEORY

A. Coherent energy manipulation

In neutron interferometer experiments accompanied by two radio-frequency (rf) oscillating fields, the total state consists of the neutron state $|\Psi_N\rangle$ and two rf fields, $|\alpha_\omega\rangle$ and $|\alpha_{\omega/2}\rangle$ represented by coherent states: $|\Psi_{\text{tot}}\rangle = |\alpha_\omega\rangle \otimes |\alpha_{\omega/2}\rangle \otimes |\Psi_N\rangle$ [23]. Coherent energy manipulation is accomplished by the interaction with an oscillating magnetic field: This scheme is depicted in Fig. 1. A polarized neutron enters an area of a spatially distributed guide magnetic field, $B_0(\mathbf{r})$, which induces a shift of potential energy, $\Delta E_{\text{pot}} = \pm\mu B_0$ ($\pm$ corresponds to parallel and antiparallel spin states and μ is the neutron magnetic moment), as a result of the Zeeman effect. This is accompanied by a change of kinetic energy: the total energy, given by the sum of kinetic and potential energies, is conserved. (The total energy is conserved during an interaction that has

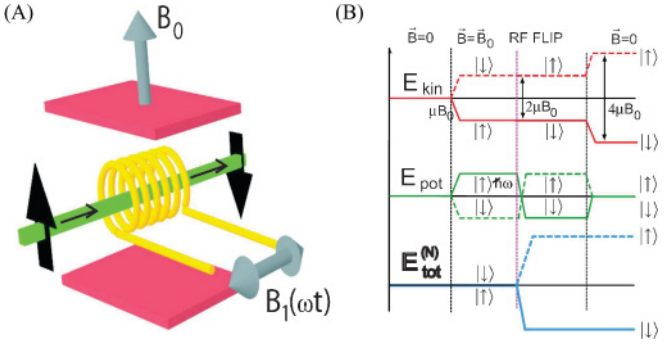

FIG. 1. (Color online) Coherent energy manipulation at a spin flip with an oscillating magnetic field. (A) At the spin flip, the energy of the neutron is coherently manipulated with the interaction of an oscillating magnetic field. (B) Energy diagrams (i.e., of kinetic, potential, and total energies) of neutrons in passing through an oscillating field $B_{\rm osc}(\omega t)$ in a guide field, B_0. The spatially distributed potential $\mu B_0(r)$ induces changes of only kinetic and potential energies. In contrast, the time-dependent interaction leads to no change of kinetic and changes of potential energy, which results in changes of total energy.

only spacial dependence [26].) Then, the spin is flipped by an additional oscillating magnetic field $B_{\rm osc}(\omega t) = B_1 \cos(\omega t + \phi)$ in a constant guide field B_0, which, in turn, leads to coherent (total) energy manipulation. In contrast to the time-independent spatial interaction [an interaction with a spatially distributed potential induced by $\mu B_0(\mathbf{r})$], a time-dependent interaction induces changes in the potential energy and the kinetic energy is kept constant. It is worth noting here that although the spin flip occurs in manipulating the total energy, the spin itself can be flipped, or rather arbitrarily manipulated, independently with the use of stationary magnetic field, for example, by a dc coil. This fact implies that a spin flip by an rf flipper accompanied by another spin flip by a dc flipper afterward or beforehand effectively works as a (total) energy manipulation without altering the spin: the spin and energy degrees of freedom in our experiments are independently manipulable.

B. State preparation

In the experiment, the incident neutron is polarized to up, denoted by $|\uparrow\rangle$. The individual states, corresponding to the spin, path, and energy degrees of freedom, are represented by a Bloch-sphere description in Fig. 2: The states of the incident neutron can be represented by the north-pole points on the sphere. In passing through the first plate (the beam splitter) of the interferometer, the state describing the neutron's path is transformed into a 50:50 superposition of path I ($|\mathrm{I}\rangle$) and path II ($|\mathrm{II}\rangle$) states. Therefore, the corresponding state lies on the equator of the path Bloch sphere. In the interferometer, a rf spin flipper operating with frequency ω is inserted in path II, where the spin-flip process by a time-dependent interaction induces energy transitions from the initial energy state $|E_0\rangle$ to states $|E_0-\hbar\omega\rangle$ by photon exchange: up spin $|\uparrow\rangle$ in path II is flipped to down spin $|\downarrow\rangle$, thus losing energy by $\hbar\omega$ [27]. Consequently, one can generate neutrons in a triply entangled GHZ-like state, given by

$$\left|\Psi_N^{\rm GHZ}\right\rangle = \frac{1}{\sqrt{2}}[|\uparrow\rangle \otimes |\mathrm{I}\rangle \otimes |E_0\rangle + |\downarrow\rangle \otimes |\mathrm{II}\rangle \otimes |E_0 - \hbar\omega\rangle]. \tag{1}$$

Note that this GHZ-like state represents a superposition of two product states: $|\uparrow\rangle \otimes |\mathrm{I}\rangle \otimes |E_0\rangle$, where all individual states are on the north poles, and $|\downarrow\rangle \otimes |\mathrm{II}\rangle \otimes |E_0 - \hbar\omega\rangle$, where all states are located on the south poles of the Bloch spheres. Here, the state of neutrons is characterized by three (spin, path, and energy) degrees of freedom, which are simply described by two-level quantum systems such as

$$\begin{cases} |\Psi_s\rangle = \{|\uparrow\rangle, |\downarrow\rangle\} \\ |\Psi_p\rangle = \{|\mathrm{I}\rangle, |\mathrm{II}\rangle\} \\ |\Psi_e\rangle = \{|E_0\rangle, |E_0 - \hbar\omega\rangle\}. \end{cases} \tag{2}$$

In this simple description, all subspaces are effectively spanned by two orthogonal bases. It is worth noting here that the energy subspace, in principle, does not consist of two discrete levels but has a continuous structure.

C. Phase manipulation

The important operations of each degree of freedom in the experiments are phase manipulations between each of two bases.

(i) The spin phase α is adjusted by a magnetic field oriented along the quantization axis (i.e., +z direction) tuned by an "accelerator" dc coil. In reality, the change of the Larmor frequency $\Delta\omega_L$ results in a phase shift $\alpha = \Delta\omega_L T_1$, where T_1 is the propagation time through the accelerator coil.

(ii) The phase manipulation of the path subspace is accomplished with the use of an auxiliary phase shifter made of a parallel-sided Si plate 5 mm thick. In this case, the phase shift χ is given by $\chi = -Nb_c\lambda D$, with the atom density N, the coherent scattering length b_c, the wavelength of the beam λ, and the thickness of the plate D.

(iii) There is a suitable method for a phase manipulation of the energy degree of freedom, which is known as a zero-field precession [28]: when two rf flippers (operated at a frequency ω_r) are set in serial, the former induces the energy difference $\pm\hbar\omega_r$ until the latter, resulting in the phase difference $\gamma = 2\omega_r T_2$, where T_2 is the propagation time between the flippers. In particular, an experimentally convenient method to manipulate individually the Larmor phase and the zero-field phase γ was found and reported in Ref. [24].

D. Mermin-like inequality

Since perfect correlations (or anticorrelations) cannot be observed in real experiments, one should use an inequality in order to clarify peculiarities of the triply entangled GHZ-like state. Mermin analyzed the GHZ argument in detail and derived an inequality suitable for experimental tests to distinguish between predictions of QM and LHVTs [16]. Assuming a tripartite system and taking the assumption in the conditionally independent form (represented by Eq. (5) in [16]) due to NCHVTs instead of LHVTs, one can obtain the border for a sum of expectation values of certain product

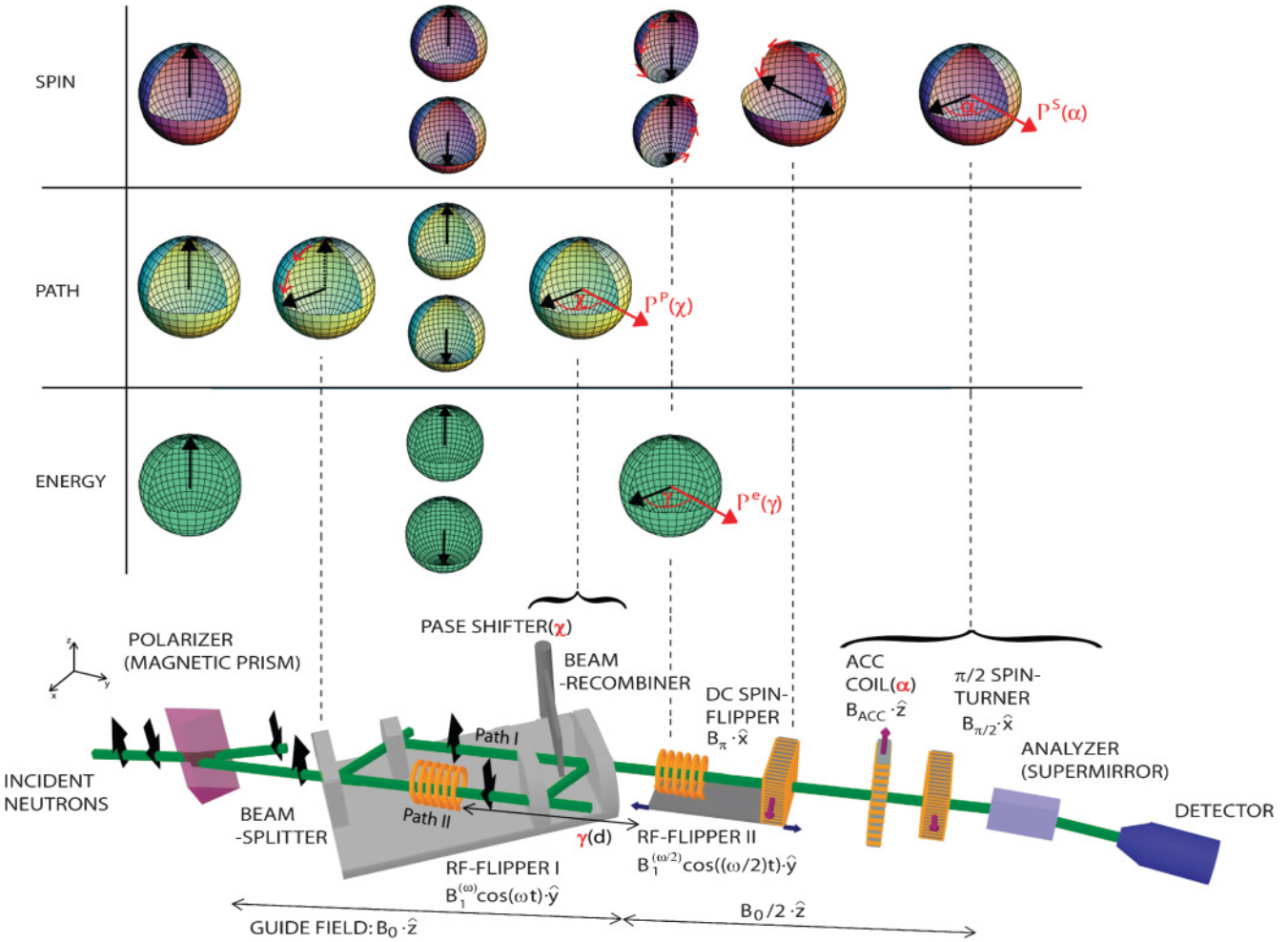

FIG. 2. (Color online) Schematic view of the main experimental setup (not to scale) for the preparation and analysis of triply entangled states in a single-neutron system together with Bloch-sphere descriptions to depict evolutions of each quantum state (i.e., the spin, path, and energy degrees of freedom). The experiment consists of three stages. (i) Preparation of a triply entangled GHZ-like state $|\Psi_N^{\mathrm{GHZ}}\rangle$: the state of neutron is the 50:50 superposition of $|\uparrow\rangle \otimes |\mathrm{I}\rangle \otimes |E_0\rangle$ (all states on the north poles) and $|\downarrow\rangle \otimes |\mathrm{II}\rangle \otimes |E_0 - \hbar\omega\rangle$ (all states on the south poles of the Bloch spheres). (ii) Manipulation of the relative phases followed by projection measurements: The directions of the projection measurements P^j are depicted by thick red arrows in Bloch spheres. (iii) Detection: Numbers of neutrons $N(\chi;\alpha;\gamma)$ are counted.

observables, which can be tested in the experiment. The sum of expectation values of product observables, called M, is defined as

$$M = E\left[\sigma_x^s \sigma_x^p \sigma_x^e\right] - E\left[\sigma_x^s \sigma_y^p \sigma_y^e\right] - E\left[\sigma_y^s \sigma_x^p \sigma_y^e\right] - E\left[\sigma_y^s \sigma_y^p \sigma_x^e\right], \tag{3}$$

where $E[\cdots]$ represents expectation values and σ_j^s, σ_j^p, and σ_j^e represent Pauli operators for the two-level systems in the spin, path, and energy degrees of freedom, respectively. NCHVTs set a strict limit for the maximum possible value of 2 ($|M| \leqslant 2$). In contrast, quantum theory predicts an upper bound of 4: Any measured value of M that is larger than 2 decides in favor of quantum contextuality. A violation up to a factor of 2 is expected with a triply entangled GHZ-like state $|\Psi_N^{\mathrm{GHZ}}\rangle$.

In order to test the Mermin-like inequality, one should determine four expectation values for joint measurements of three (i.e., spin, path, and energy) observables. We decided to extend the strategy used in the measurement of the Peres-Mermin proof of the Kochen-Specker theorem [29,30]: successive measurements of three degrees of freedom are carried out. (In addition, we are using a fair-sampling hypothesis.) Measurements of the Pauli operators in practice are realized by decomposing them into two projection operators:

$$\begin{cases} \sigma_x^l = \hat{P}^l(0) - \hat{P}^l(\pi) \\ \sigma_y^l = \hat{P}^l(\pi/2) - \hat{P}^l(3\pi/2), \end{cases} \tag{4}$$

where $l = s, p,$ and e represents spin, path, and energy components and the projection operators $\hat{P}^s(\phi)$, $\hat{P}^p(\phi)$, and $\hat{P}^e(\phi)$ are given by projectors to the states $(|\uparrow\rangle + e^{i\phi}|\downarrow\rangle)/\sqrt{2}$, $(|\mathrm{I}\rangle + e^{i\phi}|\mathrm{II}\rangle)/\sqrt{2}$, and $(|E_0\rangle + e^{i\phi}|E_0 - \hbar\omega\rangle)/\sqrt{2}$, respectively. Note that these projection operators, realized in the experiments, differ only in phase between the two orthogonal states, which is experimentally very convenient since one only needs phase manipulations: Directions of all projection measurements are depicted by thick red arrows in Bloch spheres in Fig. 2 (they all lie on the equatorial plane). In practice, the projection operators are realized at the last plate of the interferometer for the path, at the second rf spin flipper

for the energy, and at the spin analyzer for the spin. Each expectation value is determined by a combination of eight count rates in a single detector with appropriate phase settings, for instance,

$$E\left(\sigma_x^s\sigma_y^p\sigma_y^e\right) = \langle\Psi|[\hat{P}^s(0)-\hat{P}^s(\pi)]\left[\hat{P}^p\left(\frac{\pi}{2}\right)-\hat{P}^p\left(\frac{3\pi}{2}\right)\right]\left[\hat{P}^e\left(\frac{\pi}{2}\right)-\hat{P}^e\left(\frac{3\pi}{2}\right)\right]|\Psi\rangle$$
$$= \frac{N\left(0:\frac{\pi}{2}:\frac{\pi}{2}\right)-N\left(\pi:\frac{\pi}{2}:\frac{\pi}{2}\right)-N\left(0:\frac{3\pi}{2}:\frac{\pi}{2}\right)\cdots+N\left(0:\frac{3\pi}{2}:\frac{3\pi}{2}\right)-N\left(\pi:\frac{3\pi}{2}:\frac{3\pi}{2}\right)}{N\left(0:\frac{\pi}{2}:\frac{\pi}{2}\right)+N\left(\pi:\frac{\pi}{2}:\frac{\pi}{2}\right)+N\left(0:\frac{3\pi}{2}:\frac{\pi}{2}\right)\cdots+N\left(0:\frac{3\pi}{2}:\frac{3\pi}{2}\right)+N\left(\pi:\frac{3\pi}{2}:\frac{3\pi}{2}\right)}, \quad (5)$$

where $N(\alpha:\chi:\gamma)=\langle\Psi|\hat{P}^s(\alpha)\cdot\hat{P}^p(\chi)\cdot\hat{P}^e(\gamma)|\Psi\rangle$ denotes the count rate with the spin phase α, the path phase χ, and the energy phase γ.

III. EXPERIMENT AND DISCUSSION

The experiment was carried out at the perfect-crystal neutron-interferometer beam line S18 at the high-flux reactor at the Institute Laue Langevin (ILL). A schematic view of the main components of the experimental setup together with a Bloch-sphere description depicting evolutions of each degree of freedom is shown in Fig. 2. A silicon perfect-crystal monochromator was placed in the neutron guide to monochromatize the incident neutron beam to a mean wave length of $\lambda_0 = 1.92$ Å with the monochromaticity $\Delta\lambda/\lambda_0 \approx 0.01$. The cross section of the incident beam was confined to $5\times5\,\mathrm{mm}^2$. Magnetic prisms were used to polarize the incident beam vertically, before the beam enters a triple-Laue (LLL) interferometer. The interferometer was adjusted to give 220 reflections. A parallel-sided Si plate was used as a phase shifter to tune the phase χ for the path degree of freedom. This phase shifter accompanied by the beam recombination in the interferometer enabled us to realize a projection measurement with the operator $\hat{P}^p(\chi)$.

A fairly uniform magnetic guide field, B_0, in $+\hat{z}$ (~20 G), was applied around the interferometer by a pair of water-cooled Helmholtz coils (not shown in Fig. 2). The first rf spin flipper was located in this region, and its operational frequency was tuned to 58 kHz. The GHZ-like state of neutrons $|\Psi_N^{\mathrm{GHZ}}\rangle$ was generated by turning on this rf spin flipper. Along the flight path after the interferometer, another fairly uniform magnetic guide field, B_0' (at half strength, ~10 G), was applied with another pair of water-cooled coils in Helmholtz geometry (also not depicted in Fig. 2). The second rf spin flipper, tuned to the operational frequency of 29 kHz, was placed in this region. This rf spin flipper was mounted on a common translator together with a dc spin flipper. The translation of the common basis allows one to tune the phase γ of the energy degree of freedom independently [24]; for instance, $\gamma = 0, \pi/2, \pi, 3\pi/2$ resulted in implementing $\hat{P}^e(0)$, $\hat{P}^e(\pi/2)$, $\hat{P}^e(\pi)$, and $\hat{P}^e(3\pi/2)$. Note that the second rf spin flipper, in practice, worked as an energy "recombiner" described as $\hat{O}^{(\mathrm{E})} = \frac{1}{\sqrt{2}}|E_0-\hbar\omega/2\rangle(\langle E_0|+\langle E_0-\hbar\omega|)$. A spin analyzer in the $+\hat{z}$ direction (a magnetically saturated bent Co-Ti supermirror) together with a $\pi/2$ spin turner enabled the selection of neutrons in the x–y plane (normal to the quantization axis). An accelerator coil, oriented in $B_{\mathrm{acc}}+\hat{z}$, was used to adjust the spin phase $\alpha = 0,\ \pi/2,\ \pi,\ 3\pi/2,$

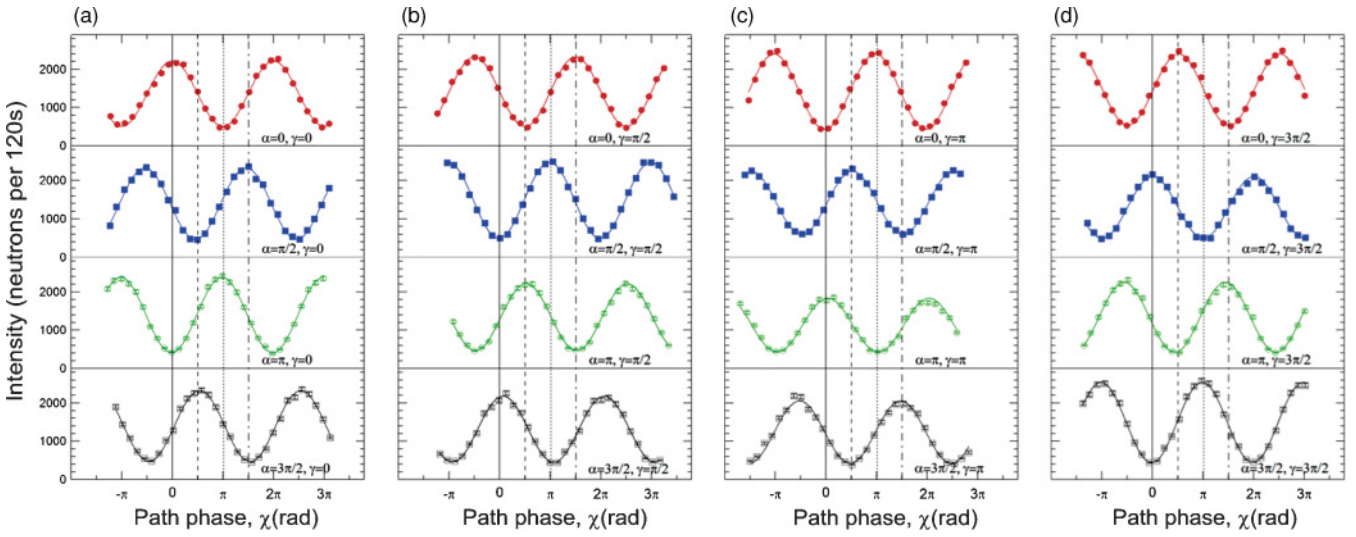

FIG. 3. (Color online) Typical intensity modulations obtained by varying the path phase χ. The phases α and γ, for the spin and the energy, respectively, are tuned at 0, $\pi/2$, π, and $3\pi/2$ in order to accomplish projection measurements of $\hat{P}(0)$, $\hat{P}(\pi/2)$, $\hat{P}(\pi)$, and $\hat{P}(3\pi/2)$ for (a) $\gamma = 0$, (b) $\gamma = \pi/2$, (c) $\gamma = \pi$, and (d) $\gamma = 3\pi/2$, and in each γ setting α was set at 0, $\pi/2$, π, and $3\pi/2$ (upper to lower panels).

TABLE I. Experimentally determined expectation values and the resulting M value.

Observables	Variables α	χ	γ	Values
$\sigma_x^s\sigma_x^p\sigma_x^e$	$0, \pi$	$0, \pi$	$0, \pi$	0.659(2)
$\sigma_x^s\sigma_y^p\sigma_y^e$	$0, \pi$	$\pi/2, 3\pi/2$	$\pi/2, 3\pi/2$	−0.632(2)
$\sigma_y^s\sigma_x^p\sigma_y^e$	$\pi/2, 3\pi/2$	$0, \pi$	$\pi/2, 3\pi/2$	−0.603(2)
$\sigma_y^s\sigma_y^p\sigma_x^e$	$\pi/2, 3\pi/2$	$\pi/2, 3\pi/2$	$0, \pi$	−0.664(2)
$M = 2.558 \pm 0.004$				

accomplishing projection measurements of $\hat{P}^s(0)$, $\hat{P}^s(\pi/2)$, $\hat{P}^s(\pi)$, and $\hat{P}^s(3\pi/2)$.

By tuning the spin phase α and the energy phase γ each at 0, $\pi/2$, π, and $3\pi/2$, sixteen independent path phase χ scans (i.e., oscillation measurements) were carried out for the determination of M in Eq. (3). Typical oscillations are depicted in Fig. 3: Intensities at indicated lines ($\chi = 0, \pi/2, \pi, 3\pi/2$) were used to determine the related expectation values. The contrasts of the oscillations were just below 70%, which was about the same as those with the empty interferometer and showed that all parameters could be manipulated effectively.

Measured intensity oscillations were fitted to sinusoidal curves by the least squares method, and the four related expectation values were extracted. Statistical errors were estimated to ± 0.001 taking all fit errors from single measurement curves into account. One set of measurements consists of thirty-two oscillation measurements. (We recorded intensities with and without spin flips at each phase shifter χ position, which allowed estimation and correction, if necessary, of the path-phase χ instability afterward.) We measured four sets of thirty-two oscillations to reduce statistical errors. We noticed that the statistical errors here are much smaller than those obtained in the Bell-like inequality experiments [12]. This is because the points used to determine expectation values are in the vicinity of the flat maxima or minima, for example, $N(\alpha = 0, \pi : \chi : \gamma = 0, \pi)$ around $\chi = 0, \pi$ on the solid and dotted lines in Fig. 3, which reflects robustness of the Mermin-like inequality and led to rather small statistical errors. Four measurements were summed up as weighted averages, and the final value and the error were determined. So, the final errors are the sum of systematic and statistical errors. (Systematic errors were mainly due to the path-phase χ instability, that is, unwanted drifts of the χ phase, during the measurement.) We obtained four expectation values listed in Table I together with settings of variables and the final M value. In evaluating the Mermin-like inequality, M was calculated to be $M = 2.558 \pm 0.004$. This exhibits a clear violation, $M \not\leqslant 2$, of the noncontextual border. The reduction from the ideal value of 4 is solely due to reduced contrast of the interference term from the interferometer, that is, just below 70%.

Our results with neutrons were obtained with detectors of more than 99% efficiency. This experiment alone will not close all loopholes (e.g., a light-cone loophole still remains), but such a high efficiency of detectors for neutrons will help in the study of the physics of contextuality. The use of entanglement of the energy degree of freedom is not limited to neutrons but is easily applicable to other quantum systems. Furthermore, a coherent manipulation of the energy degree of freedom can be extended to create artificial multilevel quantum systems (e.g., of the order of 10^3) in a single-particle system by applying a multiple-frequency energy-manipulation scheme in serial. Such a system could be used for quantum information processing.

IV. CONCLUSIONS

We have demonstrated the violation of the Mermin-like inequality with the use of three, (spin, path, and energy) degrees of freedom in a single-neutron system. The concept of entanglement is not limited between spatially separated systems but also is generally applicable between degrees of freedom. Here, as a realization of triple entanglement in a single-particle system, the GHZ-like state was generated and analyzed. Now we are ready to investigate other triply entangled states, for instance, the W state [31], which is expected to be generated rather easily with a double-loop neutron interferometer [32].

ACKNOWLEDGMENTS

We thank A. Cabello (Sevilla) and A. Hosoya (Tokyo) for their critical readings of the manuscript and appreciate discussions with C. Brukner, E. Balcar, J. Klepp (Vienna), and S. Filipp (Zurich). This work has been supported partly by the Japanese Science and Technology Agency and the Austrian Fonds zur Föderung der Wissenschaftlichen Forschung (No. P21193-N20 and Hertha-Firnberg-Program T389-N16).

[1] A. Einstein, A. Podolsky, and N. Rosen, Phys. Rev. **47**, 777 (1935).
[2] J. S. Bell, Physics **1**, 195 (1964); J. F. Clauser and A. Shimony, Rep. Prog. Phys. **41**, 1881 (1978).
[3] R. A. Bertlmann and A. Zeilinger, eds., *Quantum [Un]speakables* (Springer Verlag, Berlin, 2002).
[4] For instance, A. Aspect, J. Dalibard, and G. Roger, Phys. Rev. Lett. **49**, 1804 (1982); G. Weihs, T. Jennewein, C. Simon, H. Weinfurter, and A. Zeilinger, *ibid.* **81**, 5039 (1998).
[5] For instance, M. A. Rowe, D. Kielpinski, V. Meyer, C. A. Sackett, W. M. Itano, C. Monroe, and D. J. Wineland, Nature (London) **409**, 791 (2001); D. N. Matsukevich, P. Maunz, D. L. Moehring, S. Olmschenk, and C. Monroe, Phys. Rev. Lett. **100**, 150404 (2008).
[6] D. L. Moehring, M. J. Madsen, B. B. Blinov, and C. Monroe, Phys. Rev. Lett. **93**, 090410 (2004); **93**, 109903 (2004).
[7] H. Sakai, T. Saito, T. Ikeda, K. Itoh, T. Kawabata, H. Kuboki, Y. Maeda, N. Matsui, C. Rangacharyulu, M. Sasano, Y. Satou, K. Sekiguchi, K. Suda, A. Tamii, T. Uesaka, and K. Yako, Phys. Rev. Lett. **97**, 150405 (2006).
[8] S. Kochen, and E. P. Specker, J. Math. Mech. **17**, 59 (1967).
[9] N. D. Mermin, Rev. Mod. Phys. **65**, 803 (1993).

[10] B. R. La Cour, Phys. Rev. A **79**, 012102 (2009).
[11] S. Basu, S. Bandyopadhyay, G. Kar, and D. Home, e-print arXiv:quant-ph/9907030; Phys. Lett. A **279**, 281 (2001).
[12] Y. Hasegawa, R. Loidl, G. Badurek, M. Baron, and H. Rauch, Nature **425**, 45 (2003).
[13] E. Amselem, M. Rådmark, M. Bourennane, and A. Cabello, Phys. Rev. Lett. **103**, 160405 (2009).
[14] D. M. Greenberger, M. A. Horne, and A. Zeilinger, in *Bell's Theorem, Quantum Theory, and Conceptions of the Universe*, edited by M. Kafatos (Kluwer Academic, Dordrecht, 1989), p. 73.
[15] D. M. Greenberger, M. A. Horne, A. Shimony, and A. Zeilinger, Am. J. Phys. **58**, 1131 (1990).
[16] N. D. Mermin, Phys. Rev. Lett. **65**, 1838 (1990).
[17] J. W. Pan, D. Bouwmeester, M. Daniell, H. Weinfurter, and A. Zeilinger, Nature **403**, 515 (2000).
[18] Z. Zhao, Y. A. Chen, A. N. Zhang, T. Yang, H. J. Briegel, and J. W. Pan, Nature **430**, 54 (2004).
[19] C. A. Sackett, D. Kielpinski, B. E. King, C. Langer, V. Meyer, C. J. Myatt, M. Rowe, Q. A. Turchette, W. M. Itano, D. J. Wineland, and C. Monroe, Nature **404**, 256 (2000).
[20] A. Rauschenbeutel, G. Nogues, S. Osnaghi, P. Bertet, M. Brune, J.-M. Raimond, and S. Haroche, Science **288**, 2024 (2000).
[21] Y. Hasegawa, R. Loidl, G. Badurek, M. Baron, and H. Rauch, Phys. Rev. Lett. **97**, 230401 (2006).
[22] Y. Hasegawa, R. Loidl, G. Badurek, S. Filipp, J. Klepp, and H. Rauch, Phys. Rev. A **76**, 052108 (2007).
[23] S. Sponar, J. Klepp, R. Loidl, S. Filipp, G. Badurek, Y. Hasegawa, and H. Rauch, Phys. Rev. A **78**, 061604(R) (2008).
[24] S. Sponar, J. Klepp, G. Badurek, and Y. Hasegawa, Phys. Lett. A **372**, 3153 (2008).
[25] H. Rauch, and S. A. Werner, *Neutron Interferometry* (Clarendon, Oxford, 2000).
[26] For instance, L. I. Schiff, *Quantum Mechanics*, 3rd ed. (McGraw-Hill, Tokyo, 1968).
[27] J. Summhammer, Phys. Rev. A **47**, 556 (1993).
[28] R. Golub, R. Gähler, and T. Keller, Am. J. Phys. **62**, 779 (1994).
[29] A. Cabello, S. Filipp, H. Rauch, and Y. Hasegawa, Phys. Rev. Lett. **100**, 130404 (2008).
[30] H. Bartosik, J. Klepp, C. Schmitzer, S. Sponar, A. Cabello, H. Rauch, and Y. Hasegawa, Phys. Rev. Lett. **103**, 040403 (2009).
[31] W. Dür, G. Vidal, and J. I. Cirac, Phys. Rev. A **62**, 062314 (2000).
[32] S. Filipp, Y. Hasegawa, R. Loidl, and H. Rauch, Phys. Rev. A **72**, 021602(R) (2005).